POLITECNICO
MILANO 1863

SCUOLA DI INGEGNERIA INDUSTRIALE
E DELL'INFORMAZIONE

EXECUTIVE SUMMARY OF THE THESIS

Quantification of atrial fluid-dynamic from 4D Flow PC-MRI: development of a software tool and application to the study of patients affected by Anderson Fabry disease

TESI MAGISTRALE IN BIOMEDICAL ENGINEERING – INGEGNERIA BIOMEDICA

AUTHOR: Jacopo Rossi

ADVISOR: Emiliano Votta, Alessandra Riva

ACADEMIC YEAR: 2020-2021

1. Introduction

The left atrium (LA) is the upper chamber of the left heart and its function is to convey oxygenated blood into the left ventricle (LV) through the mitral valve. The LA plays three different functions in three phases of the cardiac cycle: 1) *reservoir*, storing the venous return during the isovolumetric LV contraction; 2) *conduit*, transferring passively blood to LV 3) *active contraction*, contracting and contributing 15-30% to LV stroke volume(1).
Fabry disease, or Anderson-Fabry disease (AFD), is a rare genetic disease related to the X recessive chromosome. It is a multiple-organ disease that causes the accumulation of sphingolipids in the lysosome, damaging the involved organs. One of the most damaged organs is the heart. The initial cardiac involvement is detected by cardiac magnetic resonance (MR) with contrast agent techniques that quantify the T1 parameter, i.e., the longitudinal relaxation time, which gives information about interstitial and diffused fibrosis (**Figure 1**).

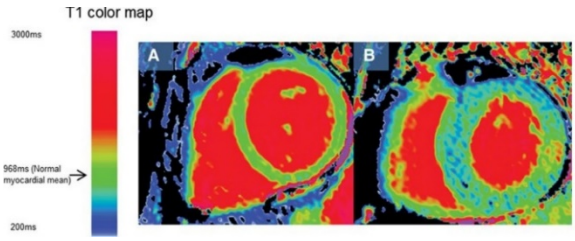

Figure 1 Mapping of T1 parameter in a healthy subject (A) and in a AFD patient (B).

In case of cardiac involvement, LV hypertrophy (LVH) is one of the most common complications, affecting more than the 50% of male patients. It causes LV wall thickening and pressure elevation within the heart and may result in poor pumping action.
Even if AFD mostly affects the LV, the LA is also affected by sphingolipids accumulation. Boyd *et al.*(2) showed how LA enlargement in AFD patients occurs before LVH. A direct consequence is an increase in LA wall stiffness and thus a decrease in LA compliance.

This work aimed to developing a tool to evaluate the fluid-dynamics within the LA in AFD patients and to characterize potential AFD-related alterations. A graphical user interface (GUI) was developed for LA segmentation from *cine* CMR images, borrowing and adapting a pre-existing method developed for LV. A second GUI was developed for the post-processing of 4D Flow CMR data, adapting existing functions and adding new ones. 4D Flow CMR is a phase-contrast imaging technique that allows, with a suitable post-processing, the comprehensive quantification of fluid dynamics inside the heart, including those parameters related to the inherent 3D nature of LA blood flow.

The indexes computed and evaluated for the purpose of this work were: 1) kinetic energy (KE) and its rotational component (RKE); 2) Viscous energy loss (EL), i.e., the portion of KE lost because of frictional viscous forces; 3) Vortex Volume (volume of blood involved in vortical structures); 4) Wall shear stress (WSS) on the LA walls.

2. Methods

2.1 Study population

Two populations were analyzed: patients affected by AFD (n=8) and healthy subjects (n=6). AFD patients had different degrees of cardiac involvement: LVH (n=2), no LVH but decreased T1 values (n=5), no LVH and normal T1 values (n=1). Subjects' characteristics are summarized in Table 1.

	HC (n=6)	**AFD** (n=8)	***p* value**
Age [yr]	41±12	42±13	0.89
Sex (M:F)	4:2	5:3	0.61
BSA [m²]	1.9±0.3	1.8±0.2	0.55
Height [m]	1.8±0.1	1.7±0.1	0.15
Weight[kg]	74.9±21.2	71.9±8.4	0.72

Table 1 Characteristics of the two populations, data are represented as mean ± SD. BSA, body surface area.

2.2 MRI Acquisition

Images used for the LA segmentation and fluid-dynamic analysis were acquired using a 1.5 T Magnetom Aera (Siemens, Erlangen, Germany) scanner. During the same session, *cine* CMR images and 4D Flow data were acquired. *Cine* CMR images included short axis (SAx) and long axis (LAx) views of the left heart. 4D Flow data were acquired with retrospective ECG-gating with parasagittal orientation to cover up the entire heart.

2.3 Image Analysis

The LA segmentation method consisted in an adaptation of a previously implemented method for LV (3). In a GUI, the user has to segment the LA in two steps. In the first one, the LA is segmented in the available LAx views: in the first acquired frame, the LA endocardial contour, the position of mitral valve and the position of the highest points in the left atrium are traced in every available view. An Optical Flow algorithm then tracks in time the traced contours.

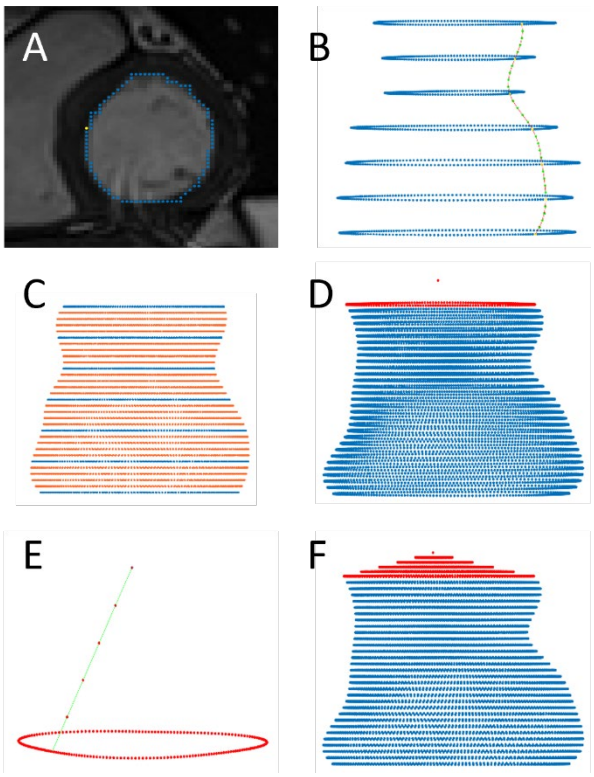

Figure 2 A: section of a SAx view and its contoure, traced by the user. B: every section of SAx view resampled, the spline shows how correspondent points are joined up. C: section of SAx with the addition of dummy points between consecutive slices. D: in red the points used for the terminal part reconstruction, the last segmented section, and the highest point. E: method for the terminal part reconstruction, a line is traced from every point of the last segmented section to the highest points, points are then resampled on dummy planes between the last slice and the highest point. F: result of the reconstruction.

In the second step, at the first acquired frame the LA contour is traced on SAx views that includes

the LA (identified by the mitral valve position and by the highest LA point from LAx segmentation). Tracing can be manual or automatic, and again an Optical Flow algorithm is used to track the LA contour in time. The user can then navigate the performed segmentation in space and time and, if needed, correct it. From the points obtained from LAx and SAx segmentation, the software creates the 3D geometry of LA. If the SAx stack covers the entire LA, the SAx segmentation points are re-sampled and dummy points are added between consecutive SAx slices (**Figure 2**). If some SAx slices are missing, the information coming from LAx segmentation and the available SAx are exploited. The available SAx segmentation for one slice is projected onto the missing SAx and shrinked according to the endocardial tracing from LAx segmentation (**Figure 3**). This procedure is performed for every acquired time frame until the entire LA is reconstructed. Once the reconstruction is over, the fitting steps as those described before.

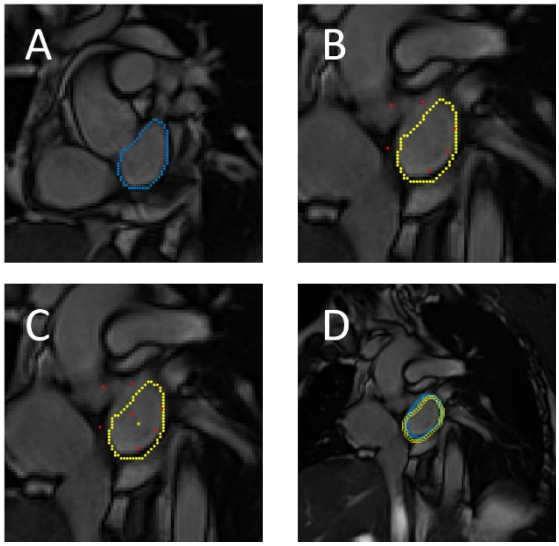

Figure 3 A: segmentation of SA slices. B: in yellow the projection of the previous slice's points, in red two points from every LAx view, these points are the ones with the closest z to the z of the slice. C: points of the top right figure and their barycenter. D: in yellow the profile reconstructed with the developed method, in blue the real one.

At the end of the fitting procedure, the points laying below the mitral valve are deleted and the remaining point cloud is registered and overlapped with the 4D Flow acquired volume. Finally, a 3D binary mask of LA is built, with value 1 for points inside the LA, and 0 elsewhere.

2.4 Hemodynamic indexes

For every subject the following parameters were calculated from the LA binary mask:

Kinetic Energy: computed at each time frame as:

$$KE = \sum_{i=1}^{N} \frac{1}{2} \rho_{blood} V_i v_i^2 \qquad \textbf{Eq. 1}$$

where N is the total number of voxels inside the LA, v is the velocity of the voxel and V is the voxel volume and ρ_{blood} is blood density (considered constant and equal to 1025 kg/m^3).

Rotational Kinetic Energy: computed for each time frame following the procedure of Arvidsson *et al.*(4). First, the instantaneous atrial center of mass was determined and the angular momentum around the center of mass was computed using the position and the velocity vectors. The total angular momentum was obtained through summation of all voxels. The direction of total angular momentum and the position of atrial center of mass were used to determine the axis of rotation. RKE around this axis was computed as:

$$RKE = \sum_{i=1}^{N} \frac{1}{2} I_i \omega_i^2 \qquad \textbf{Eq. 2}$$

where ω is the angular velocity of the voxel and I the moment of inertia of the voxel, computed approximating the voxel to a material point.

Viscous Energy Loss: the rate of viscous energy losses was computed as:

$$\dot{EL}_{tot} = \mu_{blood} \sum_{w=1}^{N} \phi_v V_w \qquad \textbf{Eq. 3}$$

where ϕ_v is the viscous dissipation function per unit volume obtained from the Navier Stokes energy balance equation, and μ_{blood} is blood viscosity. Blood was considered both as a Newtonian fluid wit constant blood viscosity and as a non-Newtonian fluid (Quemada model), with viscosity depending on subject hematocrit and shear rate. EL was computed as the time integral of $\dot{EL}$.

Wall Shear Stress: under the assumption of Newtonian blood behavior, the shear component of the stress tensor was computed as:

$$\tau_{ij} = \mu_{blood} \left(\frac{\partial u_i}{\partial x_j} + \frac{\partial u_j}{\partial x_i} \right) \text{with } i \neq j \qquad \textbf{Eq. 4}$$

Where *i,j* are the space axes, and *u* is the velocity. The computation of this parameter was based on the *Global Volumetric* approach (5). Velocity at the wall was set to 0, then all the velocity data within an interval of $3 \cdot voxelsize$ from the boundary were eliminated. The remaining velocity data, included the 0 values, were used to interpolate the new velocity data. The interpolation function was then evaluated at the boundary points. Velocity derivatives were computed through the application of Sobel filters, for every point of the boundary the inward normal unit vector was computed. WSS magnitude was computed based on the derivative components of the velocity and the inward normals.

Vortical Structures: vortical structures were computed using two methods: the λ_2 method, largely used in vortex detection in the heart that depends on the threshold select by the user, and the Ω method (6), a third-generation method that is not sensitive to threshold variations.

For the λ_2 method, the following steps were followed (7): 1) computation of the velocity gradient tensor; 2) computation of its symmetric (S) and anti-symmetric (W) component; 3) computation of the eigenvalues (λ_1,λ_2,λ_3) of $S^2 + W^2$; 4) identification of λ_2, where $\lambda_1 < \lambda_2 < \lambda_3$; 5) identification of a *patient-specific* threshold, all the voxels with $\lambda_2 < \overline{\lambda_2}/2$ (where $\overline{\lambda_2}$ is the mean value of all $\lambda_2 < 0$) are considered; 6) vortices were defined as those with a volume $> V_{voxel}$, with a connectivity neighbor-hood region analysis applied to include only collections of interconnected voxels, i.e., sharing of≥4 voxels.

For the Ω method, W Ω was computed as:

$$\Omega = \frac{||W||_F^2}{||S||_F^2 + ||W||_F^2 + \epsilon} \qquad \text{Eq. 5}$$

where $||\cdot||_F$ is the Froebenius norm, and $\epsilon = 0.001 \times (b-a)_{max}$, with $b = ||W||_F^2$ $a = ||S||_F^2$, is a parameter to limit the noise's effect. This method does not require a specific threshold, the only condition to apply is to set $\Omega > 0.50$, many users proved that a proper threshold is $\Omega > 0.52$. Then the vortex identification follows the same procedure as for λ_2.

2.5 Statistical analysis

Statistical analyses were performed with GraphPad Prism 9 (GraphPad Software, San Diego, CA, USA); a p-value of <0.05 was considered significant. Normality distribution of data was assessed through Shapiro-Wilk test. Comparisons between populations were evaluated through un-paired tests: t-test for normally distributed data, Mann-Whitney t-test otherwise.

3. Results

Energetic Analysis: all energetic parameters (KE, RKE and EL) were quantified at peak systole, at first diastolic peak (peak E-wave, rapid ventricular filling) and at second diastolic peak (peak A-wave, atrial active contraction). To compare LAs with different volume, every parameter was normalized with respect to the LA volume in the relevant time frame. The time-course of KE and RKE was comparable with the one found in literature (4), with three distinct peaks in systole, and at the E-wave and A-wave peaks, respectively (**Figure 4**). Between the two populations, no statistically significant differences were found (**Table 2**).

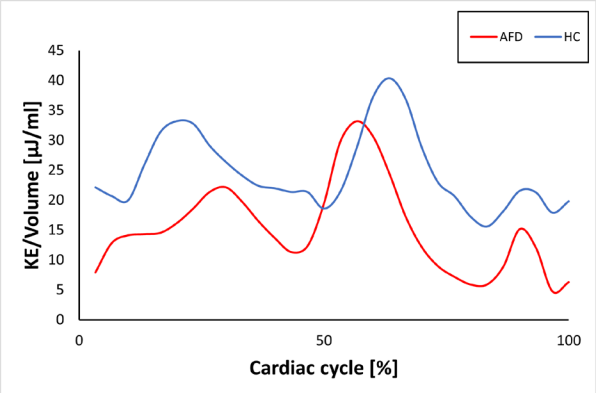

Figure 4 Evolution of kinetic energy during the cardiac cycle, AFD in red, HC in blue.

	HC (n=6)	AFD (n=8)	*p* value
KEs [µJ/ml]	22±7	21[13; 25]	0.13
KEE [µJ/ml]	34±10	31±7	0.72
KEA [µJ/ml]	15[11;33]	14[7;17]	0.70
RKEs [µJ/ml]	13±4	11±5	0.43
RKEE [µJ/ml]	17±6	15[9;16]	0.68
RKEA [µJ/ml]	8±2	6±3	0.70
RKE/KE [%]	51±6	47±7	0.40

Table 2 Values of KE and RKE normalized respect to the volume, in [ml]. Data are represented as mean ± SD for normal distribution case and as median [IQR] for non-normal distribution case.

A similar time-course was observed for the rate of viscous energy loss. No statistically significant difference between the two populations were detected in terms of EL nor $\dot{EL}$. However, for AFD, when comparing peak $\dot{EL}$ values obtained considering blood as a Newtonian vs. non-Newtonian fluid statistically significant differences were found, with higher values detected using the Quemada model (**Table 3**).

	Newtonian (n=6)	Quemada (n=8)	*p* value
EL_S[μW/ml]	6.7±1.5	8.1±1.7	0.0004
$\dot{EL}_E$[μW/ml]	8.4±2.7	9.5±2.6	0.0003
EL_A[μW/ml]	5.6±2.0	6.7±2.3	0.0008

Table 3 Values of $\dot{EL}$ normalized by the volume. Data are expressed as mean ± SD. S=systolic peak; E=wave E; A=wave A.

Vortical Structures: vortex volumes were evaluated at the three characteristic peaks (systolic, E-wave and A-wave) with both methods. Vortex volumes were comparable between the two populations. Also, there were no statistically significant differences between the application of the two methods (**Table 4**).

	λ_2 (n=8)	Ω (n=8)	*p* value
V_S [cm³]	10.07±2.84	11.46±4.46	0.37
V_E [cm³]	9.91[8.65;11.46]	10.76±3.50	0.85
V_A [cm³]	9.33[6.99;10.49]	10.31±3.13	0.14

Table 4 Values of vortex volumes (V), expressed in [cm³]. Data are represented as mean ± SD for normal distribution case and as median [IQR] otherwise. S=systolic peak; E=wave E; A=wave A.

Wall Shear Stress: the time-averaged WSS magnitude over the cardiac cycle was computed. No significant differences were found between the two populations (**Table 5**).

	HC (n=6)	AFD (n=8)	*p* value
WSS_S [mPa]	140±40	120±30	0.46
WSS_E [mPa]	110±21	100±15	0.74
WSS_A [mPa]	100±20	90±15	0.14

Table 5 Values of time-averaged WSS, expressed in [mPa]. Data are expressed in mean ± SD.

4. Discussion

Results must be considered as preliminary, because of the small sample size and the heterogeneity of cardiac involvement in AFD patients considered for this study.

4.1. Discussion of the results

From the energetic analysis no significant difference emerged. However, slightly lower KE values were noticed in AFD patients during the diastolic peak. This might be caused by a reduced atrial compliance in AFD patients (2). Moreover, the ratio KE/RKE slightly decreased in AFD patients (47% *vs* 51%), possibly due to a reduced twisting activity in AFD LA (2). In AFD patients, values of the viscous dissipation rate were slightly lower than in controls, and this may be due to an altered velocity field in the LA. The comparison between Quemada and Newtonian models shows that a more patient-specific computation of viscosity lead to higher viscous dissipation rates, both at systolic and diastolic peaks, with statistically significant differences, although patterns during the cardiac cycle remain similar between the two methods.

The analysis of the vortical structures shows that the two methods lead to results with no statistically significant differences. However, the Ω method was not yet tested for the computation of vortex in the heart. According to Garcia *et al.*(7), the λ_2 method identifies higher vortex volumes during the first diastolic peak than during the systolic peak.

WSS analysis does not show any significant difference between the two populations, as for KE and viscous energy loss values are a little higher in HC with respect to AFD.

4.2. Conclusions

The absence of statistically significant differences between the two populations might be because in AFD population most of the subjects do not have relevant cardiac involvement (6 over 8 without LVH), showing similar characteristic to the LA of healthy subjects. However, possible alterations in LA blood flow might become detectable once the pathology worsens. This hypothesis might be confirmed with further studies on a larger population, for the 3 subgroups (no LVH and no lower T1, no LVH and lower T1, LVH).

4.3. Innovations, limitations, and future developments

The innovation in this thesis concerns the development of a segmentation tool for the LA and the reconstruction of a 3D dynamic mask of the LA, with the purpose of 4D Flow data analysis. The development of this tool allowed the analysis of hemodynamic variables that, following deeper analysis, could have clinical relevance in the study and stratification of Anderson Fabry disease. The possibility to reconstruct the LA domain, also when short axis slices are missing, makes this tool more flexible.

The main limitations are the sample size and the software used for programming. MATLAB is a good development tool, thanks to the large number of functions already implemented, however it has limitations related to data storage and computational efficiency. Moreover, an expert operator is always required to use the software. The translation of the MATLAB code in another programming language could improve the tool; the release of a standalone executable may improve its usability by clinical end users.

Bibliography

1. Blume GG, McLeod CJ, Barnes ME, Seward JB, Pellikka PA, Bastiansen PM, et al. Left atrial function: Physiology, assessment, and clinical implications. Vol. 12, European Journal of Echocardiography. 2011. p. 421–30.
2. Boyd AC, Lo Q, Devine K, Tchan MC, Sillence DO, Sadick N, et al. Left atrial enlargement and reduced atrial compliance occurs early in fabry cardiomyopathy. Journal of the American Society of Echocardiography. 2013 Dec;26(12):1415–23.
3. Strambi Laura, Zocchi Gregory, Votta Emiliano, Riva Alessandra. Un nuovo strumento di analisi della fluidodinamica intraventricolare da dati di 4D Flow PC-MRI: sviluppo e applicazione preliminare allo studio delle anomalie associate a rimodellamento ventricolare. 2019.
4. Arvidsson P, Toger J, Heiberg E, Carlsson M, Arheden H. Quantification of left and right atrial kinetic energy using four-dimensional intracardiac magnetic resonance imaging flow measurements. Journal of Cardiovascular Magnetic Resonance. 2013 Jan;15(S1).
5. Piatti F, Pirola S, Bissell M, Nesteruk I, Sturla F, della Corte A, et al. Towards the improved quantification of in vivo abnormal wall shear stresses in BAV-affected patients from 4D-flow imaging: Benchmarking and application to real data. Journal of Biomechanics. 2017 Jan 4;50:93–101.
6. Liu C, Gao Y sheng, Dong X rui, Wang Y qian, Liu J ming, Zhang Y ning, et al. Third generation of vortex identification methods: Omega and Liutex/Rortex based systems. Journal of Hydrodynamics. 2019 Apr 1;31(2):205–23.
7. Garcia J, Sheitt H, Bristow MS, Lydell C, Howarth AG, Heydari B, et al. Left atrial vortex size and velocity distributions by 4D flow MRI in patients with paroxysmal atrial fibrillation: Associations with age and CHA2DS2-VASc risk score. Journal of Magnetic Resonance Imaging. 2020 Mar 1;51(3):871–84.